Colorimetric Logic Gates Based on Poly(2-alkyl-2-oxazoline)-Coated Gold Nanoparticles

*Victor R. de la Rosa, Zhiyue Zhang, Bruno G. De Geest, and Richard Hoogenboom**

A straightforward end-capping strategy is applied to synthesize xanthate-functional poly(2-alkyl-2-oxazoline)s (PAOx) that enable gold nanoparticle functionalization by a direct "grafting to" approach with citrate-stabilized gold nanoparticles (AuNPs). Owing to the presence of remaining citrate groups, the obtained PAOx@AuNPs exhibit dual stabilization by repulsive electrostatic and steric interactions giving access to water soluble molecular AND logic gates, wherein environmental temperature and ionic strength constitute the input signals, and the solution color the output signal. The temperature input value could be tuned by variation of the PAOx polymer composition, from 22 °C for poly(2-^{n}propyl-2-oxazoline)@AuNPs to 85 °C for poly(2-ethyl-2-oxazoline)@AuNPs. Besides, advancing the fascinating field of molecular logic gates, the present research offers a facile strategy for the synthesis of PAOx@AuNPs of interest in fields spanning nanotechnology and biomedical sciences. In addition, the functionalization of PAOx with xanthate offers straightforward access to thiol-functional PAOx of high interest in polymer science.

1. Introduction

Gold nanoparticles (AuNPs) constitute a rapidly growing research area, which has led to applications spanning nanotechnology,[1] biotechnology,[2] catalysis, and sensing,[3] due to their distinctive properties with respect to those of the bulk metal solid. AuNPs exhibit a strong localized surface plasmon resonance (SPR) due to the collective coherent oscillation of conduction band electrons across the nanoparticle upon interaction with light at a specific resonant wavelength. The shape and frequency of the SPR band depends on the size and shape of the particle, as well as on the dielectric properties of the medium surrounding the nanoparticle. The shifts in the SPR band, or the corresponding color variation associated to a change in the AuNP microenvironment have been exploited as an analytical output signal to develop ultrasensitive bioanalyte detection and diagnostics.[4] As a result, AuNPs represent an ideal platform to translate molecular events into logic systems with a large impact on the color properties of the solution, therefore allowing to replicate Boolean logic gates on a molecular scale. These colorimetric systems are particularly attractive for point-of-use detection and diagnostics applications, and to construct memory elements of sequential logic operations with the ability to store information.[4c,5]

Chemical tuning of the AuNP surface is necessary to impart water-solubility, biological compatibility, and specificity to the nanoparticles. In general, AuNPs are stabilized by electrostatic (with ligands such as carboxylates, amines or pyridine)[6] or by steric interactions. Stabilization of AuNPs with polymers has been widely investigated as an attractive strategy to stabilize AuNPs and also to confer the polymer properties to the final polymer@AuNP constructs.[7] In this context, antifouling AuNPs have been produced by functionalization with polyethylene glycol (PEG) for the development of drug/gene delivery vectors and as contrast agents,[2a,8] although some concerns about their applicability in vivo are arising.[9] Similarly, stimuli-responsive AuNPs have been produced through functionalization with thermoresponsive polymers such as PNIPAm[10] or poly(oligoethylene glycol) methacrylates.[11] These temperature responsive systems are of high interest in colorimetry due to the high sensitivity derived from the large absorption extinction coefficient of AuNPs that usually stands ca. three orders of magnitude beyond that of organic dyes. Poly(2-alkyl-2-oxazoline)s (PAOx) have been proposed as suitable alternatives to PEG and moreover their thermal-responsiveness can be easily tuned by variation of the alkyl substituent in the 2-oxazoline monomer.[12] However, despite the potential of PAOx for the preparation of stimuli-responsive nanoparticles, the research on PAOx-coated AuNPs has remained on hold since the pioneering work of Jordan et al.,[13] who developed a grafting-from methodology. In the present work, a new facile strategy is developed for the synthesis of PAOx@AuNPs via a grafting-to approach. As recently found for PNIPAm@AuNPs,[14] these PAOx@AuNPs exhibit dual stabilization by both repulsive electrostatic and steric interactions (see **Figure 1**).[15] The PAOx@AuNPs remained insensitive to temperature changes in the absence of an electrolyte to screen the nanoparticle's negative charges, whereas aggregation was observed in the presence of an electrolyte only beyond the

Dr. V. R. de la Rosa, Prof. R. Hoogenboom
Supramolecular Chemistry Group
Department of Organic and Macromolecular Chemistry
Ghent University
Krijgslaan 281 S4, 9000 Ghent, Belgium
E-mail: richard.hoogenboom@ugent.be
Z. Zhang, Prof. B. G. De Geest
Department of Pharmaceutics
Ghent University
Ottergemsesteenweg 460, 9000 Ghent, Belgium

DOI: 10.1002/adfm.201404560

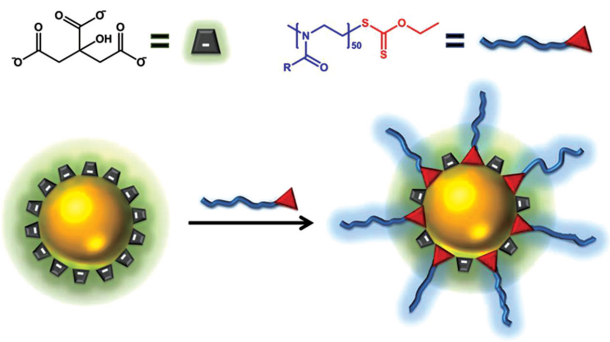

Figure 1. Schematic representation for the ligand exchange of citrate-stabilized AuNPs with xanthate-functional PAOx. The resulting poly(2-alkyl-2-oxazoline)-grafted gold nanoparticles exhibit dual stabilization by repulsive electrostatic and steric interactions.

PAOx transition temperature. This dual stabilization mechanism is exploited in this contribution for the utilization of the PAOx@AuNPs as supramolecular "AND" Boolean logic gates, by controlling temperature and electrolyte concentration as logic inputs and the color of the solution as output. In addition, variation of the alkyl-substituent of the polymer-enabled control over the temperature input value, further advancing on the promising field of AuNP-based logic gates.[5a,16]

2. Results and Discussion

2.1. Synthesis and Characterization of Xanthate-Functionalized Poly(2-alkyl-2-oxazoline)s

PAOx are readily obtained via living cationic ring-opening polymerization of 2-alkyl-2-oxazolines. Telechelic functional polymers are accessible by selection of the initiator and terminating agent (a nucleophile) in a one pot fashion.[17] Unlike other biocompatible polymers, such as poly(ethyleneglycol) PEG or temperature-responsive polymers such as PNIPAm, PAOx permit the variation of the polymer side chain hydrophobicity by gradually tuning the length of the alkyl chain in the 2-alkyl-2-oxazoline monomer (e.g., methyl, ethyl, propyl). Thereby, structure-property relationships can be evaluated by systematic variation of one single parameter (polymer side-chain hydrophobicity),[18] thus turning PAOx into an ideal polymer platform for the stabilization of AuNPs and the tuning of the nanoparticle stimuli-responsiveness. The hereby developed method for the preparation of PAOx-AuNP constructs is based on xanthate-terminated PAOx that are subsequently used to functionalize citrate-stabilized AuNPs through ligand exchange. Xanthate groups inherently adsorb to gold in a similar fashion as trithiocarbonates, which have been applied for the direct functionalization of AuNPs with polymers synthesized via RAFT polymerization.[19] Furthermore, xanthates can be easily transformed into thiols by aminolysis, making them interesting for further polymer modification and coupling.

The preparation of xanthate functionalized PAOx was envisioned by direct end-capping of the living polymer chains with the commercially available potassium ethyl xanthogenate as terminating nucleophile (see **Figure 2**, top).[20]

To study the influence of the polymer hydrophilicity on the thermal-responsiveness of the resulting PAOx@AuNPs, poly(2-methyl-2-oxazoline) (PMeOx), poly(2-ethyl-2-oxazoline) (PEtOx) and poly(2-^{n}propyl-2-oxazoline) (P^{n}PrOx) with a length of 50 repeating units were synthesized and end-capped with potassium ethyl xanthogenate, resulting in well-defined xanthate-functionalized polymers (**Table 1**). The presence of the xanthate groups at the polymer terminus was confirmed by ^{1}H-NMR spectroscopy and matrix-assisted laser desorption and ionization time of flight (MALDI-TOF) mass spectrometry, both

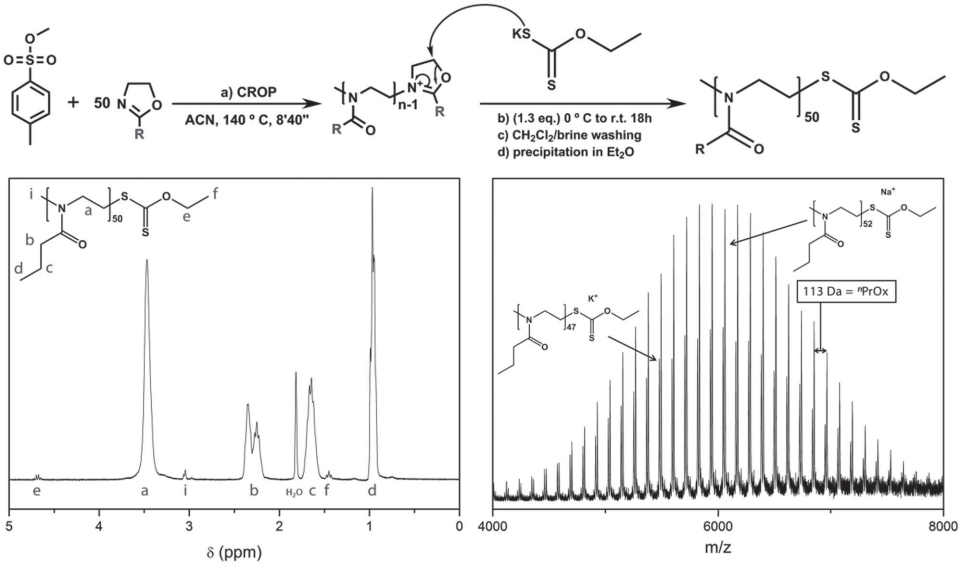

Figure 2. Top: Synthesis of xanthate-functionalized PAOx. R = CH_3–(MeOx), CH_3CH_2–(EtOx), or $CH_3CH_2CH_2$–(^{n}PrOx). Dispersities ranged from $Đ$ = 1.08 to 1.10. Bottom: ^{1}H-NMR spectrum of P^{n}PrOx50-xanthate in $CDCl_3$ (300 MHz) and corresponding MALDI-TOF mass spectrum confirming the intended polymer structure.

Table 1. Characterization of xanthate-terminated PAOx.

Polymer	DP	% Functionalization[a)]	M_n [Da]	Dispersity [$Đ$]	T_{CP}[d)] [°C]
PMeOx-xanthate	43[a)]/52[b)]	+95%	4 600[b)]/10 700[c)]	1.05[b)]/1.10[c)]	–
PEtOx-xanthate	50[a)]/50[b)]	+95%	5 000[b)]/9 400[c)]	1.04[b)]/1.08[c)]	97 / 94[e)]
P^{n}PrOx-xanthate	50[a)]/52[b)]	+95%	6 000[b)]/9 500[c)]	1.04[b)]/1.08[c)]	20 / 22[e)]

DP = degree of polymerization. [a)]Calculated based on ^{1}H-NMR spectroscopy; [b)]Calculated based on MALDI-TOF mass spectrometry; [c)]Calculated based on SEC in DMA against PMMA standards; [d)]Measured by turbidimetry in milli-Q water or [e)]in a 50×10^{-3} M NaCl solution.

showing quantitative functionalization (see Figures 2 and S1–S9, Supporting Information).

While PMeOx exhibits a hydrophilicity somewhat larger than that of PEG and is not thermoresponsive,[21] PEtOx and P^{n}PrOx exhibit a lower critical solution temperature (LCST) behavior due to their negative entropy of solvation. Turbidimetry studies were performed on 5 mg mL^{-1} polymer solutions in deionized water to quantify the phase transition temperature or cloud point temperature (T_{CP}) of the three synthesized PAOx-xanthate (see Table 1 and Figures S10–S12, Supporting Information). As expected, PMeOx$_{50}$-xanthate did not exhibit temperature responsiveness, whereas PEtOx$_{50}$-xanthate showed a cloud point of ca. 90 °C. P^{n}PrOx$_{50}$-xanthate, the polymer with the largest hydrophobicity, exhibited a T_{CP} = 20 °C, below the reported T_{CP} of 25 °C, ascribed to the presence of the xanthate hydrophobic end-group. The turbidimetry measurements were also performed in the presence of 50×10^{-3} M NaCl, yielding comparable results due to the low concentration of NaCl used.[22] Nevertheless, we will later observe a clear-cut impact of NaCl on the temperature responsiveness of PAOx-coated AuNPs (vide infra).

2.2. Synthesis and Characterization of Poly(2-alkyl-2-oxazoline)-Coated AuNPs

AuNPs were synthesized based on the aqueous method of Turkevitch and Frens, wherein citrate was used as both a reducing agent for $HAuCl_4$ and a stabilizer for the generated AuNPs, yielding citrate-stabilized AuNPs.[23] Upon reflux in aqueous medium, a deep-purple solution was obtained, containing citrate@AuNPs with an estimated mean diameter of 25 nm as measured by transmission electron microscopy (TEM). Citrate ligands, weakly bond to the nanoparticle, were subsequently displaced by addition of the xanthate-functional PAOx in aqueous medium, followed by three centrifugation-redispersion steps to remove all unbound PAOx. In analogy to dithioesters and trithiocarbonates, xanthate group coordination to gold surfaces leads to the formation of stable monolayers, thereby not requiring the previous aminolysis of the xanthate group.[11,14,19a,24] TEM measurements undoubtedly showed the presence of the PAOx coating on the surface of the AuNPs after the exchange (see **Figure 3** and S13, Supporting Information). Depending on the composition of the PAOx polymer, the observed thickness of the PAOx corona ranged from 6 to 1.5 nm as measured by TEM, being the smallest for P^{n}PrOx-coated AuNPs, indicating a lower surface coverage of the polymer. This polymer has a larger footprint due to the ^{n}propyl side chains, thus having a more condensed structure in aqueous solution during displacement of citrate.

The AuNPs were subsequently evaluated by dynamic light scattering (DLS), observing an increase in particle average diameter from 40 nm for citrate@AuNPs to 70 nm for PEtOx@AuNPs (see **Figure 4**). The observed increase in particle diameter is slightly smaller than the length of a fully stretched PAOx50 chain, of ≈18 nm. PMeOx-coated AuNPs showed a 4 nm larger mean size, possibly due to the high hydrophilicity of PMeOx that results in better-hydrated, more stretched PMeOx chains. In contrast, the more hydrophobic P^{n}PrOx-coated AuNPs exhibited a lower average diameter of 57 nm, as a consequence of chain–chain hydrophibic interactions that result in a more compact packing of the polymer brush. An additional distribution was observed in the DLS measurements, with a size below 10 nm, which was found to be an artifact due to rotational diffusion of the nanoparticles. Although rotational diffusion is usually not observed in DLS measurements, it can manifest itself when measuring nonspherical or birefringent gold particles, as has been previously reported.[25] To prove this assumption, DLS measurements were performed at two different angles (90° and 173°) and the intensity was plotted against the relaxation time, as this is angular dependent for translational diffusion but not for rotation diffusion (see Figures S14–S17, Supporting Information). In this way, we

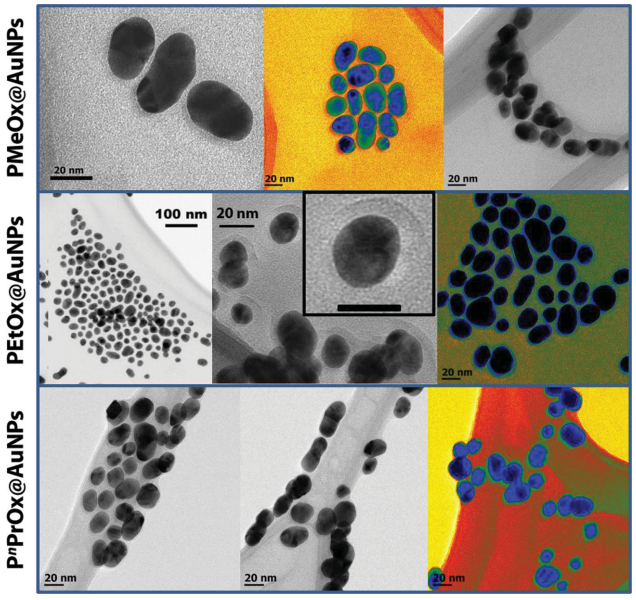

Figure 3. Bright field TEM pictures of PAOx-coated AuNPs. Some of the pictures have been colored to highlight the polymer corona around the gold nanoparticle. The inset displays one of the nanoparticles, where the PEtOx corona is clearly visible (scale bar = 20 nm).

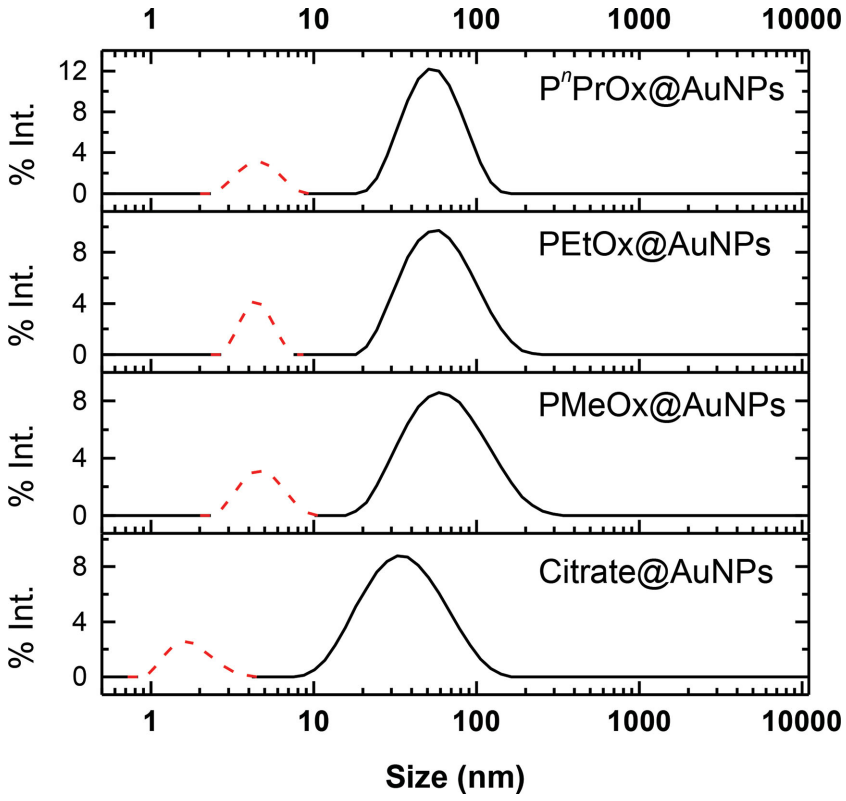

Figure 4. DLS data for the citrate@AuNPs and the PAOx@AuNPs. A clear shift in particle size is observed for all the PAOx-coated AuNPs compared with citrate@AuNPs, with a size following the order of oxazoline hydrophilicity: PMeOx > PEtOx > P^{n}PrOx. The minor distribution observed below 10 nm was proven to be an artifact due to rotational diffusion of the AuNPs. Conditions: AuNPs concentration = 0.09 mg mL^{-1} in deionized (milli-Q) water. Temperature = 25 °C. Angle = 173° (backscattering mode).

could prove that the additional size distribution results from nanoparticle rotational diffusion, as the relaxation time was independent of scattering angle. Thus, this second size distribution was not considered for determination of the nanoparticles mean size.

Next, the PAOx grafting on the AuNPs was investigated by UV–vis spectroscopy. The citrate-stabilized AuNPs showed a broad absorption with a maximum at 524 nm, corresponding to the SPR. SPR of noble metal nanoparticles is a consequence of the polarized oscillations of the electron cloud, induced by the oscillating electric field of the incident electromagnetic wave, according to Mie's theory. This phenomenon is highly sensitive to the dielectric constant of the microenvironment around the nanoparticle and therefore AuNP coverage by a polymer corona can be manifested as alterations in the SPR band.[26] Upon grafting with PAOx, the SPR band of the AuNPs is slightly broadened and red shifted, indicating the change in the dielectric constant of the microenvironment around the gold nanocore, as seen in **Figure 5**. This reflects the variation in chemical composition at the gold–water interface, and explains the observed trend in SPR band displacement, that follows the hydrophobicity order of the PAOx: P^{n}PrOx- > PEtOx- > PMeOx-grafted AuNPs. An estimation of the PAOx grafting density was made through calculation of the AuNPs molecular weight via UV–vis spectroscopy,[27] resulting in 2–4 chains nm^{-2}, in-line with previous reports on adsorption of RAFT polymers to Au surfaces[24d] (see Supporting Information). Aqueous solutions of the PAOx-coated AuNPs remained stable when kept at room temperature without showing any color change or macroscopic precipitation when kept for several days at room temperature.

2.3. Evaluation of the Temperature Responsiveness of Poly(2-alkyl-2-oxazoline)-Coated AuNPs

The thermoresponsive behavior of the PAOx-coated AuNPs was assessed by variable-temperature UV–vis spectroscopy. Interestingly, unlike the individual PAOx-xanthate polymers, PAOx-grafted AuNP solutions in demineralized water were found to be insensitive to temperature variations, even at temperatures far above the T_{CP} of the independent PAOx. As seen in **Figure 6**a–c, no change in the SPR band maximum wavelength can be observed upon heating any of the PAOx@AuNPs solutions. The slight decrease in signal intensity observed with increasing temperatures, of about 0.10 a.u., can be ascribed to solvent thermal expansion that results in a slightly lower concentration of nanoparticles. In contrast to the high stability shown by PAOx@AuNPs, citrate-stabilized AuNPs subjected to the same heating ramp exhibited a decrease in signal intensity larger than 0.7 a.u., due to partial macroscopic precipitation of the AuNPs (see Figure S18, Supporting Information).

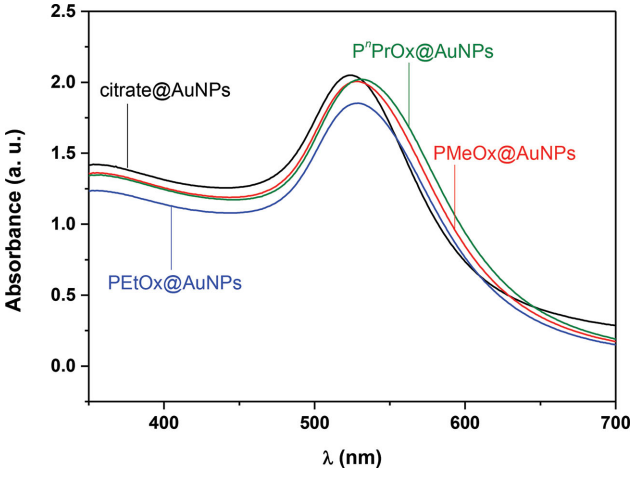

Figure 5. UV–vis spectra of the synthesized AuNPs. Upon PAOx grafting onto the AuNPs, the spectra appear broadened and slightly red shifted, following the order of polymer hydrophobicity: λ_{max}(citrate@AuNPs) < λ_{max}(PMeOx@AuNPs) < λ_{max}(PEtOx@AuNPs) < λ_{max}(P^{n}PrOx@AuNPs). Concentration: 0.1 mg mL^{-1}. Temperature = 25 °C.

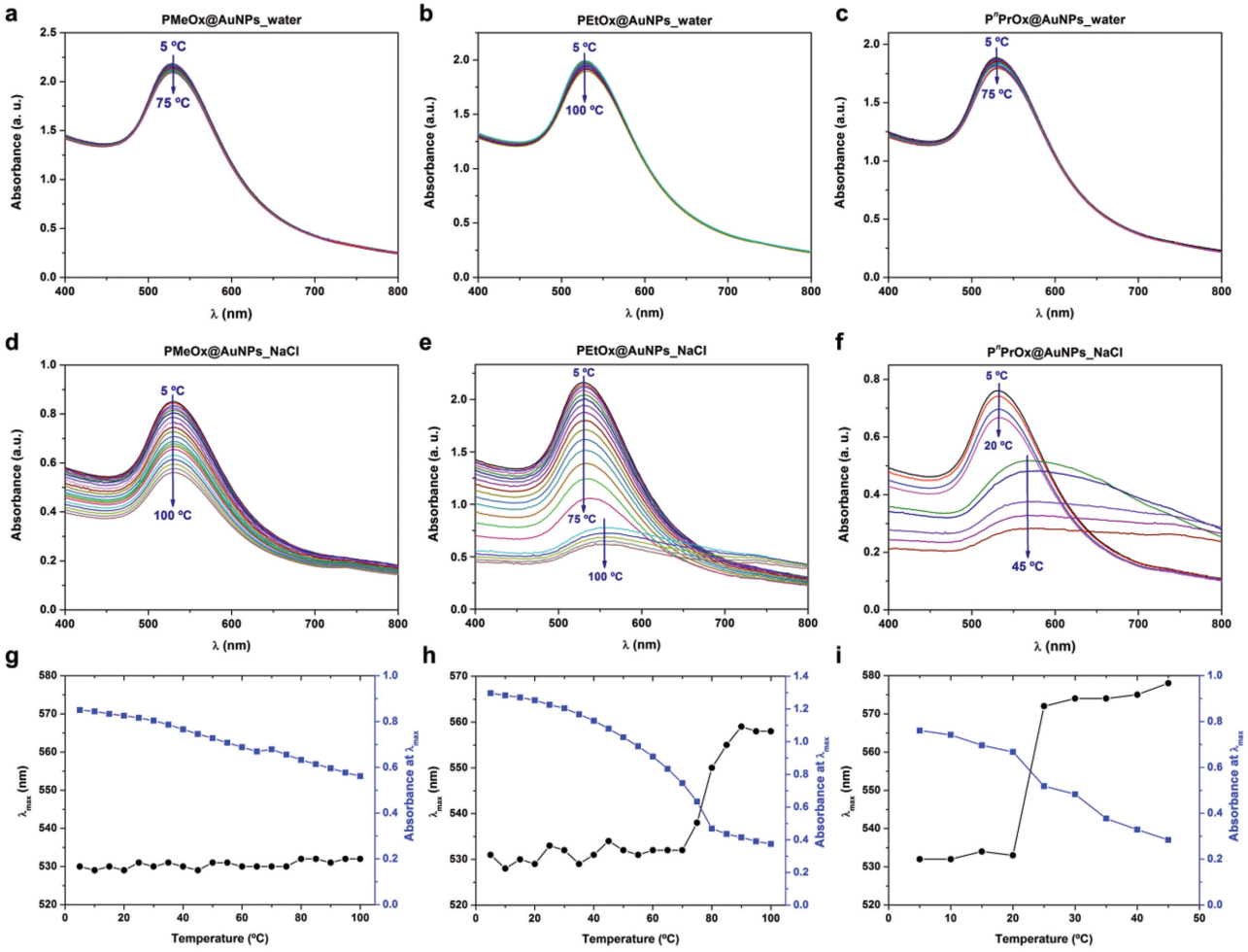

Figure 6. UV–vis spectra of the synthesized PAOx@AuNPs. a–c) UV–vis spectra upon heating the PAOx@AuNPs solutions in demineralized water (milli-Q), wherein no SPR band shift is observed. d–f) UV–vis spectra upon heating the PAOx@AuNPs solutions in the presence of NaCl 50×10^{-3} M; PMeOx@AuNPs show a decrease in absorption intensity partially due to macroscopic particle precipitation; however, no SPR band shift is observed, indicating no nanoparticle aggregation. PEtOx- and P^{n}PrOx-coated AuNPs exhibit a temperature-triggered nanoparticle aggregation, causing a shift in the SPR band of 33 nm for PEtOx@AuNPs and of 37 nm for P^{n}PrOx@AuNPs at 75–80 °C and 20–25 °C, respectively. g–i) Evolution of the SPR band maximum wavelength (λ_{max}) and the associated absorbance with increasing temperature. The temperature-triggered shift of λ_{max} is especially sharp for P^{n}PrOx@AuNPs, coinciding with the T_{CP} of the free P^{n}PrOx$_{50}$-xanthate polymer at 22 °C.

We speculate that the absence of a temperature-induced aggregation of the thermoresponsive PAOx@AuNPs was caused by electrostatic stabilization of the nanoparticles due to the remaining presence of citrate units on the surface of the AuNPs, as it was recently reported for PNIPAm-stabilized AuNPs.[14] Therefore, the variable-temperature UV–vis spectroscopy experiments were reproduced in a 50×10^{-3} M NaCl solution to screen the citrate negative charges and suppress nanoparticle stabilization due to repulsive Coulombic interactions (Figure 6d–i). PMeOx@AuNPs showed no SPR band shift upon heating, as expected from the lack of thermal-responsiveness of PMeOx. A progressive decrease of absorption intensity was nevertheless observed for PMeOx@AuNPs, due to solvent thermal expansion and a minor AuNPs macroscopic precipitation, although no appreciable difference by eye was found between the solution before and after heating. It should be noted that the addition of salt triggered partial macroscopic precipitation of the AuNPs with a lower polymer grafting density (i.e., PMeOx@AuNPs and P^{n}PrOx@AuNPs), leading to a decreased value of absorbance when compared with the PEtOx@AuNPs. Nevertheless, after this initial partial precipitation the polymer-coated AuNPs remained stable in solution.

In contrast to PMeOx@AuNPs, PEtOx- and P^{n}PrOx-coated AuNPs did exhibit a temperature-triggered aggregation, as indicated by the sharp red shift in the SPR band produced by interparticle surface plasmon coupling[28] at temperatures close to the T_{CP} of the individual PAOx. The transition temperature of PEtOx@AuNPs is suppressed by about 15 °C, which is ascribed to the increased local concentration of the polymer in combination with the high concentration dependence of the T_{CP} of PEtOx.[29] In the presence of a strong electrolyte such as NaCl, the electrostatic stabilization is suppressed and the nanoparticles were solely stabilized by the steric hindrance exerted by

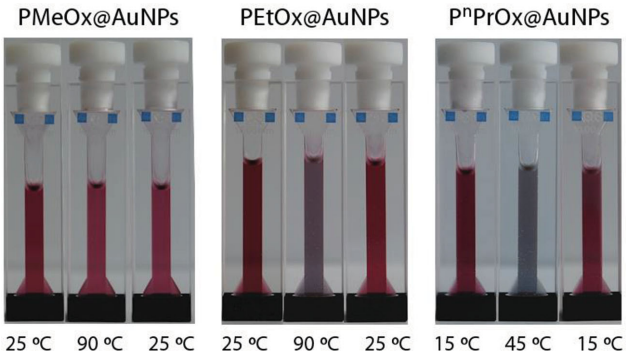

Figure 7. Photographs of PAOx-grafted AuNPs solutions in the presence of 50×10^{-3} M NaCl at temperatures below the corresponding polymer phase-transition temperatures, above, and back to the initial temperature. A clear color change is observed for the thermoresponsive PEtOx@AuNPs and P^{n}PrOx@AuNPs, whereas the solution containing PMeOx@AuNPs remains unchanged. The samples were kept at high temperature for 5 min. Concentration: 0.1 mg mL^{-1}.

the PAOx brush and thus their aggregation became governed by the LCST transition of the grafted PAOx. The temperature-induced aggregation of the PAOx@AuNPs and the subsequent shift in the SPR band resulted in a color change from violet to blue clearly visible by eye. As seen in **Figure 7**, the PAOx@AuNPs recovered they original appearance when brought back to a temperature below the polymer T_{CP}, thus demonstrating the reversibility of the transition.

The dual stabilization of the PAOx@AuNPs by both steric hindrance resulting from the PAOx brush and repulsive Coulombic interactions due to remaining citrate units was assessed by zeta potential measurements. As seen in **Table 2**, citrate@AuNPs showed a zeta potential of ≈ –40 mV, while PAOx@AuNPs ζ_{pot} values were in the range of –25 mV, indicating the presence of sufficient remaining citrate groups on the nanoparticle surface to render effective stabilization via repulsive electrostatic interactions. Upon PAOx@AuNPs dispersion in a 50×10^{-3} M $NaCl_{aq}$ solution, the citrate negative charges became screened by the Na^+ ions of the electrolyte, and the zeta potential values dropped to ≈ –5 mV, which is insufficient for electrostatic stabilization. While citrate@AuNPs immediately aggregated in 50×10^{-3} M $NaCl_{aq}$ resulting in macroscopic precipitation, PAOx@AuNPs remained stable and, in the case of PEtOx- and P^{n}PrOx-grafted AuNPs, became susceptible to changes on the environmental temperature.

The stability of the PAOx-stabilized AuNPs in the presence of NaCl was assessed by monitoring the evolution of the PAOx UV–vis spectrum isothermally below their transition temperature. A progressive decrease in overall intensity was observed as a consequence of nanoparticle precipitation. This decay was nevertheless very slow, constituting a maximum of 10% decrease in nanoparticle concentration after 17 h (see Figures S19–S21, Supporting Information) and, importantly, did not lead to a shift in the SPR band and in the associated solution color. PMeOx@AuNPs exhibited the highest stability, due to the high hydrophilicity of PMeOx.

2.4. Colorimetric Logic Gates Based on Poly(2-alkyl-2-oxazoline)-Coated AuNPs

The dual stabilization of PAOx@AuNPs by steric and electrostatic interactions was further exploited to use temperature and solution ionic strength as inputs for a molecular logic gate. As schematically depicted in **Figure 8** (top), increasing the temperature beyond the PAOx T_{CP} (input 1) results in a collapse of the polymer by virtue of its LCST behavior. However, PAOx@AuNP aggregation is impeded by the remaining electrostatic repulsive forces, leading to invariability of the solution appearance. Similarly, the addition of NaCl (input 2) produces the screening of the citrate negative charges on the surface of the AnNP, suppressing Coulombic stabilization, but aggregation is now impaired by the PAOx brush repulsive steric interactions. Therefore, both inputs need to be simultaneously applied to obtain an output solution color change, corresponding to a logical conjunction or AND gate (see logic table in Figure 8). Interestingly, selection of the PAOx composition granted control over the value of the temperature input, from 22 °C for P^{n}PrOx@AuNPs to 80 °C for PEtOx@AuNPs.

3. Conclusion

Xanthate-functional PAOx were synthesized, allowing direct grafting to citrate-stabilized AuNPs. The obtained PAOx@AuNPs exhibited dual stabilization by repulsive electrostatic and steric interactions giving access to water soluble molecular AND logic gates, wherein environmental temperature and ionic strength constitute the input signals, and the solution color the output. Furthermore, the temperature input value could

Table 2. Characterization of PAOx-functionalized gold nanoparticles.

AuNP	Size[a] [nm]	$\zeta_{pot.}$ (water)[b] [mV]	$\zeta_{pot.}$ (NaCl)[b] [mV]	T_{CP}[c] [°C]	λ_{max}[d] [nm]
Citrate@AuNPs	40.2 ± 20.6	–42.3	–	–	524
PMeOx@AuNPs	73.4 ± 34.2	–26.5	–5.7	–	527
PEtOx@AuNPs	69.7 ± 35.7	–25.2	–8.6	80[d]	529–562[e]
P^{n}PrOx@AuNPs	57.3 ± 21.2	–23.9	–4.6	22[d]	532–569[e]

[a]Mean particle size, calculated by DLS (0.1 mg mL^{-1} in water); [b]Zeta potential measurements performed on 0.1 mg mL^{-1} AuNPs solutions in milli-Q water or in 50×10^{-3} M NaCl aqueous solution; [c]Transition temperature (AuNP aggregation) measured by temperature-dependent UV–vis spectroscopy in 50×10^{-3} M NaCl aqueous solution. The AuNP transition temperature can be selected by tuning PAOx composition; [d]λ_{max} calculated by UV–vis spectroscopy (0.1 mg mL^{-1} in 50×10^{-3} M $NaCl_{aq}$) below the T_{CP} and [e]above.

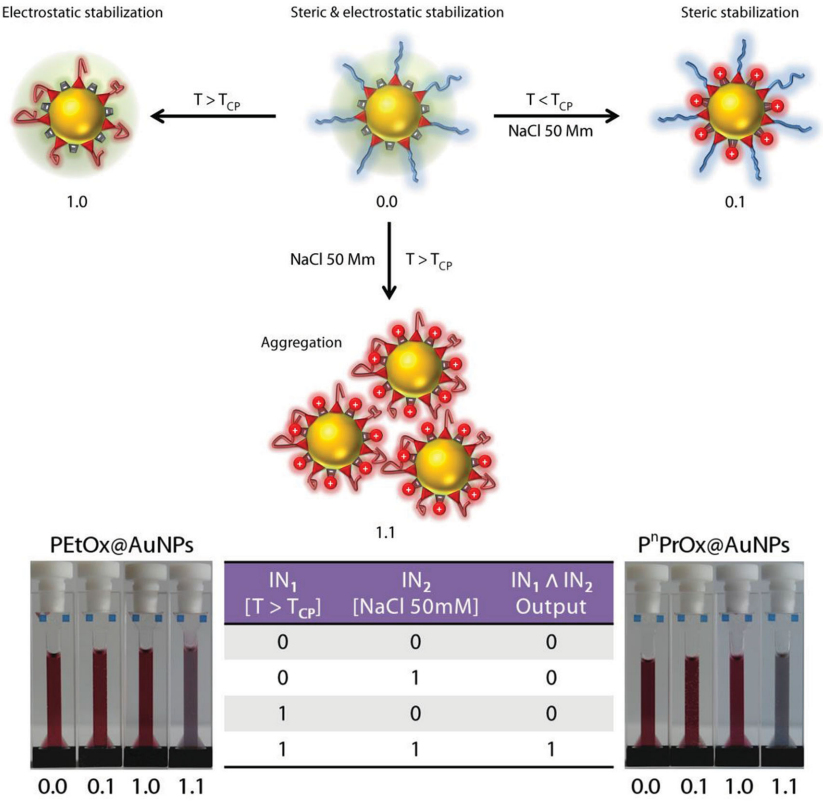

IN_1 [$T > T_{CP}$]	IN_2 [NaCl 50mM]	$IN_1 \wedge IN_2$ Output
0	0	0
0	1	0
1	0	0
1	1	1

Figure 8. Top: Schematic representation of the working mechanism of the PAOx@AuNP–based AND gate. Bottom: Logic table of the AND gate. Input 1: Temperature above PAOx transition temperature. Input 2: NaCl 50×10^{-3} M. The shift in the SPR band occurs only if both inputs are true, with the consequent color change observed. The pictures show PEtOx@AuNPs and P^{n}PrOx@AuNPs solutions corresponding to the four possible input combinations. T_{CP} (PEtOx@AuNPs) = 80 °C. T_{CP} (P^{n}PrOx@AuNPs) = 22 °C. Concentration = 0.10 mg mL^{-1}.

be tuned by variation of the PAOx polymer composition, from 22 to 85 °C for P^{n}PrOx@AuNPs and PEtOx@AuNPs, respectively. Besides advancing in the fascinating field of molecular logic gates, the present research offers a facile strategy for the synthesis of PAOx@AuNPs of interest in fields spanning nanotechnology and biomedical sciences. Moreover, functional initiators and monomers may be used in future work to render multifunctional PAOx@AuNPs with high potential in biotechnology. In addition, xanthate-functionalized PAOx can be easily converted into thiol-functional PAOx with many postmodification possibilities being of high interest in polymer science.

4. Experimental Section

Synthesis of Poly(2-alkyl-2-oxazoline)-Xanthate: Methyl tosylate (MeOTs, Aldrich) was distilled prior to use. 2-Methyl-2-oxazoline, 2-ethyl-2-oxazoline (EtOx, Aldrich), and 2-^{n}propyl-2-oxazoline (^{n}PrOx, synthesized as previously reported[30] were distilled over barium oxide (BaO, Aldrich). Acetonitrile (CH_3CN, Acros) was dried over molecular sieves (3Å). All reagents were stored and handled under dried nitrogen in a glovebox (Vigor gas purification technologies, Inc.). The polymerizations were performed in capped vials in a single mode microwave Biotage initiator 60 (IR temperature sensor). A 4 M solution of the 2-alkyl-2-oxazoline monomer was prepared in acetonitrile in the presence of 1/50 equivalents of methyl tosylate. The polymerization mixture was heated to 140 °C in the microwave synthesizer for 8 min 40 s, calculated according to the previously reported kinetics,[31] cooled to 0 °C and the living polymer chains were terminated by addition of 1.3 equivalents potassium ethyl xanthogenate (Aldrich) under a dry nitrogen atmosphere. The polymerization mixture was kept stirring for 18 h at room temperature after which, the solvent was evaporated under reduced pressure. PEtOx-xanthate and P^{n}PrOx-xanthate were redissolved in dichloromethane and washed three times with water and brine to remove the excess of potassium ethyl xanthogenate. The organic phase was dried over anhydrous magnesium sulphate, filtered and the polymer precipitated in cold diethyl ether, obtaining a white powder that was filtered and dried in a vacuum oven at 30 °C for 24 h. The PMeOx–xanthate polymerization mixture was purified by dialysis against demineralized water (Spectra Por dialysis tubing, Mwt. cut-off 1000 Da), freeze-dried and subsequently precipitated in cold diethyl ether from dichloromethane. The polymers were characterized by ^{1}H-NMR spectroscopy in $CDCl_3$ in a Bruker Avance 300 MHz spectrometer. Size exclusion chromatography (SEC) measurements were performed in an Agilent 1260-series equipped with a 1260 ISO-pump, a 1260 Refractive Index Detector (RID), and 2 × PL-GEL Mixed-D 300 × 7.5 mm columns in series inside a 1260 Thermostated Column Compartment (TCC) at 50 °C. The used solvent was DMA containing 50×10^{-3} M of LiCl to suppress interactions between the analyte and the packing material, such as adsorption or ion-exchange (flow rate of 0.5 mL min^{-1}). The molar masses were calculated against PMMA standards. MALDI-TOF mass spectrometry analysis were performed on an Applied Biosystems Voyager-DE STR instrument equipped with nitrogen laser operating at 337 nm, pulsed-ion extraction source and reflectron detector. The laser pulse width is 3 ns with a maximum power of 20 Hz. Spectra were recorded in reflector mode with an acceleration voltage of 20 kV and delay of 400 ns. 100 single shot acquisitions were summed to give the spectra and the data were analyzed using Data Explorer software. Samples were prepared by dissolving the matrix 2-(4-hydroxyphenylazo) benzoic acid (HABA) in acetone (20 mg mL^{-1}), mixing with the polymer (1 mg/mL) and sodium iodide in acetone (5 mg mL^{-1}) used as cationizing agent. Milli-Q water was obtained from a Sartorius Arium 611 with a Sartopore 2 150 (0.45 + 0.2 mm pore size) cartridge filter (resistivity less than 18.2 MΩ cm). Turbidimetry measurements were performed in a CARY Bio 100 UV–vis spectrophotometer equipped with a temperature controller, at a wavelength of 600 nm. The temperature sensor was placed in a cuvette containing the same volume of milli-Q water as the polymer solutions. Solutions of the polymers were prepared in milli-Q water or 50×10^{-3} M $NaCl_{aq}$ at 5 mg mL^{-1}. Three full heating cycles were applied with a heating/cooling rate of 1 °C min^{-1} withhold steps of 10 min. at the extreme temperatures. The cloud points are given as the 50% transmittance point during the second heating ramp.

Synthesis of Citrate-Stabilized Gold Nanoparticles: Citrate-stabilized gold nanoparticles were synthesized according to the reported literature procedures.[23a] All glassware was first washed with aqua regia and then rinsed with milli-Q water several times prior to synthesis. Briefly, 20 mL of 1×10^{-3} M HAuCl was refluxed for 30 min. Then 2 mL of 1 wt% sodium citrate was quickly added and the color of solution changed from yellow to wine red within 5 min. After cooling, the reaction solution was stored at 4 °C.

Synthesis and Characterization of Poly(2-alkyl-2-oxazoline)-Grafted Gold Nanoparticles: A total of 9 mL of a citrate-stabilized gold nanoparticles solution was mixed with 200 µL of an aqueous solution containing 8 mg of PAOx-xanthate and stirred overnight at low temperature. The resulting conjugates were three times purified by centrifugation at 4 °C and 10 000 g for 30 min followed by redispersion in pure water. The PAOx@AuNPs were characterized by transmission electron microscopy (TEM). A drop of gold nanoparticle solution was allowed to air-dry onto a Formvar-carbon-coated 200 mesh copper grid and visualized using 80 keV TEM (Jeol 1010, Japan). TEM images of the AuNPs were processed via ImageJ to determine the number average size distribution in the dry state. UV–vis spectra were acquired in a CARY Bio 100 UV–vis spectrophotometer equipped with a temperature controller. Gold nanoparticle solutions were placed in quartz cuvettes (concentration 0.1 mg mL^{-1}) and scanned in the 300–800 nm range at different temperatures. Temperatures were changed in 5 °C intervals and incubated 2 min to assure thermal equilibration. Dynamic light scattering (DLS) was performed on a Zetasizer Nano-ZS Malvern apparatus (Malvern Instruments Ltd.) using disposable cuvettes. The excitation light source was a He–Ne laser at 633 nm, and the intensity of the scattered light was measured at a 173° (backscattering mode). Measurements at a 90° scattering angle were performed in a Zetasizer Nano S90. Both methods measure the rate of the intensity fluctuation and the size of the particles is determined through the Stokes–Einstein equation ($d(H) = kT/3\pi\eta D$) where $d(H)$ is the mean hydrodynamic diameter, k is the Boltzmann constant, T is the absolute temperature, η is the viscosity of the dispersing medium, and D is the apparent diffusion coefficient. Before starting the measurements, samples were incubated at the specific temperature for at least 300 s to reach equilibrium.

Supporting Information

Supporting Information is available from the Wiley Online Library or from the author.

Acknowledgements

R.H. and V.R.R. would like to thank Ghent University for financial support via the Concerted Research Actions (Project No. BOF11/GOA/023) for financial support. R.H. and B.G.G. acknowledged FWO for funding. R.H. and V.R.R. would like to thank Prof. Niek Sanders for providing access to a Malvern Zetasizer Nano S90 for 90° DLS measurements.

Received: December 24, 2014
Revised: February 18, 2015
Published online: March 18, 2015

[1] M.-C. Daniel, D. Astruc, *Chem. Rev.* **2003**, *104*, 293.
[2] a) E. C. Dreaden, A. M. Alkilany, X. Huang, C. J. Murphy, M. A. El-Sayed, *Chem. Soc. Rev.* **2012**, *41*, 2740; b) J. Conde, A. Ambrosone, V. Sanz, Y. Hernandez, V. Marchesano, F. Tian, H. Child, C. C. Berry, M. R. Ibarra, P. V. Baptista, C. Tortiglione, J. M. de la Fuente, *ACS Nano* **2012**, *6*, 8316.
[3] K. Saha, S. S. Agasti, C. Kim, X. Li, V. M. Rotello, *Chem. Rev.* **2012**, *112*, 2739.
[4] a) R. Elghanian, J. J. Storhoff, R. C. Mucic, R. L. Letsinger, C. A. Mirkin, *Science* **1997**, *277*, 1078; b) W. Zhao, M. A. Brook, Y. Li, *ChemBioChem* **2008**, *9*, 2363; c) J. Sun, Y. Xianyu, X. Jiang, *Chem. Soc. Rev.* **2014**, *43*, 6239.
[5] a) D. Liu, W. Chen, K. Sun, K. Deng, W. Zhang, Z. Wang, X. Jiang, *Angew. Chem. Int. Ed.* **2011**, *50*, 4103; b)Y. Xianyu, Z. Wang, J. Sun, X. Wang, X. Jiang, *Small* **2014**,*10*, 4833.
[6] Y. Noda, S.-i. Noro, T. Akutagawa, T. Nakamura, *Sci. Rep.* **2014**, *4*, 3578.
[7] a)J. Pyun, T. Emrick, in *Macromolecular Engineering*, Wiley-VCH Verlag GmbH & Co. KGaA, Weinheim, Germany **2007**, p. 2409; b) I. Lilge, H. Schönherr, *Eur. Polym. J.* **2013**, *49*, 1943.
[8] Y. Cheng, A. C. Samia, J. D. Meyers, I. Panagopoulos, B. Fei, C. Burda, *J. Am. Chem. Soc.* **2008**, *130*, 10643.
[9] a) N. B. Shah, G. M. Vercellotti, J. G. White, A. Fegan, C. R. Wagner, J. C. Bischof, *Mol. Pharm.* **2012**, *9*, 2146; b) Z. He, J. Liu, L. Du, *Nanoscale* **2014**, *6*, 9017.
[10] a) J. Shan, M. Nuopponen, H. Jiang, E. Kauppinen, H. Tenhu, *Macromolecules* **2003**, *36*, 4526; b) K. Kusolkamabot, P. Sae-ung, N. Niamnont, K. Wongravee, M. Sukwattanasinitt, V. P. Hoven, *Langmuir* **2013**, *29*, 12317.
[11] C. Boyer, M. R. Whittaker, M. Luzon, T. P. Davis, *Macromolecules* **2009**, *42*, 6917.
[12] a) F. C. Gaertner, R. Luxenhofer, B. Blechert, R. Jordan, M. Essler, *J. Controlled Release* **2007**, *119*, 291; b) V. R. de la Rosa, *J. Mater. Sci: Mater. Med.* **2014**, *25*, 1211; c) K. Knop, R. Hoogenboom, D. Fischer, U. S. Schubert, *Angew. Chem. Int. Ed.* **2010**, *49*, 6288; d) O. Sedlacek, B. D. Monnery, S. K. Filippov, R. Hoogenboom, M. Hruby, *Macromol. Rapid Commun.* **2012**, *33*, 1648.
[13] R. Jordan, N. West, A. Ulman, Y.-M. Chou, O. Nuyken, *Macromolecules* **2001**, *34*, 1606.
[14] Z. Zhang, S. Maji, A. B. d. F. Antunes, R. De Rycke, Q. Zhang, R. Hoogenboom, B. G. De Geest, *Chem. Mater.* **2013**, *25*, 4297.
[15] G. Gyulai, C. B. Pénzes, M. Mohai, F. Csempesz, É. Kiss, *Eur. Polym. J.* **2013**, *49*, 2495.
[16] J. Du, S. Yin, L. Jiang, B. Ma, X. Chen, *Chem. Commun.* **2013**, *49*, 4196.
[17] M. A. Tasdelen, M. U. Kahveci, Y. Yagci, *Prog. Polym. Sci.* **2011**, *36*, 455.
[18] A. Sundaramurthy, M. Vergaelen, S. Maji, R. Auzély-Velty, Z. Zhang, B. G. De Geest, R. Hoogenboom, *Adv. Healthcare Mater.* **2014**, *3*, 2040.
[19] a) O. Tzhayik, P. Sawant, S. Efrima, E. Kovalev, J. T. Klug, *Langmuir* **2002**, *18*, 3364; b) A. B. Lowe, B. S. Sumerlin, M. S. Donovan, C. L. McCormick, *J. Am. Chem. Soc.* **2002**, *124*, 11562; c) A. E. Smith, X. Xu, T. U. Abell, S. E. Kirkland, R. M. Hensarling, C. L. McCormick, *Macromolecules* **2009**, *42*, 2958.
[20] Y. Shimano, K. Sato, S. Kobayashi, *J. Polym. Sci., Part A: Polym. Chem.* **1995**, *33*, 2715.
[21] T. X. Viegas, M. D. Bentley, J. M. Harris, Z. Fang, K. Yoon, B. Dizman, R. Weimer, A. Mero, G. Pasut, F. M. Veronese, *Bioconj. Chem.* **2011**, *22*, 976.
[22] M. M. Bloksma, D. J. Bakker, C. Weber, R. Hoogenboom, U. S. Schubert, *Macromol. Rapid Commun.* **2010**, *31*, 724.
[23] a) J. Turkevich, P. C. Stevenson, J. Hillier, *Farad. Discuss.* **1951**, *11*, 55; b) G. Frens, *Nature-Phys. Sci.* **1973**, *241*, 20.
[24] a) A. Ihs, K. Uvdal, B. Liedberg, *Langmuir* **1993**, *9*, 733; b) C.-A. Fustin, C. Colard, M. Filali, P. Guillet, A.-S. Duwez, M. A. R. Meier, U. S. Schubert, J.-F. Gohy, *Langmuir* **2006**, *22*, 6690; c) J. W. Hotchkiss, A. B. Lowe, S. G. Boyes, *Chem. Mater.* **2006**, *19*, 6; d) S. Slavin, A. H. Soeriyadi, L. Voorhaar, M. R. Whittaker, C. R. Becer, C. Boyer, T. P. Davis, D. M. Haddleton, *Soft Matter* **2012**, *8*, 118.
[25] B. N. Khlebtsov, N. G. Khlebtsov, *Colloid J.* **2011**, *73*, 118.

[26] P. I. V. T. Pradeep, A. Ashokreddy, *A Textbook of Nanoscience and Nanotechnology*, Tata McGraw-Hill Education, New Dehli **2012**.
[27] a) D. J. Lewis, T. M. Day, J. V. MacPherson, Z. Pikramenou, *Chem. Commun.* **2006**, 1433; b) X. Liu, M. Atwater, J. Wang, Q. Huo, *Colloids Surf. B. Biointerfaces* **2007**, *58*, 3.
[28] S. Srivastava, B. L. Frankamp, V. M. Rotello, *Chem. Mater.* **2005**, *17*, 487.
[29] R. Hoogenboom, H. M. L. Thijs, M. J. H. C. Jochems, B. M. van Lankvelt, M. W. M. Fijten, U. S. Schubert, *Chem. Commun.* **2008**, 5758.
[30] M. M. Bloksma, C. Weber, I. Y. Perevyazko, A. Kuse, A. Baumgärtel, A. Vollrath, R. Hoogenboom, U. S. Schubert, *Macromolecules* **2011**, *44*, 4057.
[31] F. Wiesbrock, R. Hoogenboom, M. A. M. Leenen, M. A. R. Meier, U. S. Schubert, *Macromolecules* **2005**, *38*, 5025.